Study of active regions based on multiperiod GaAsN/InAs superlattice

© A.V. Babichev[1], E.V. Pirogov[2], M.S. Sobolev[2], D.V. Denisov[2], H.A. Fominykh[2,3], A.I. Baranov[2], A.S. Gudovskikh[2], I.A. Melnichenko[2,3], P.A. Yunin[4], V.N. Nevedomsky[5], M.V. Tokarev[5], B.Ya. Ber[5], A.G. Gladyshev[1], L.Ya. Karachinsky[1], I.I. Novikov[1], A.Yu. Egorov[2,¶]

[1] ITMO University,
197101 St. Petersburg, Russia
[2] Alferov University,
194021 St. Petersburg, Russia
[3] National Research University Higher School of Economics,
190008 St. Petersburg, Russia
[4] Institute for Physics of Microstructures, Russian Academy of Sciences,
603950 Nizhny Novgorod, Russia
[5] Ioffe Institute,
194021 St. Petersburg, Russia
¶ E-mail: egorov@spbau.ru

Received August 23, 2022
Revised September 26, 2022
Accepted September 26, 2022

The results of a study of nitrogen-containing active regions based on superlattices grown on GaAs substrates are presented. Active regions based on alternating InAs and GaAsN layers were fabricated by molecular-beam epitaxy using a nitrogen plasma source. Based on the XRD analysis, the thicknesses and average composition of superlattice layers are estimated. The study of dark-field images obtained by transmission electron microscopy showed the presence of interdiffusion of InAs into GaAsN. The results of a study of the photoluminescence and electroluminescence spectra at different pump levels are presented. Efficient electroluminescence is demonstrated near 1150 nm with a full width at half-maximum of about ~ 90 meV.

Keywords: Superlattices, molecular beam epitaxy, gallium arsenide, dilute nitride, GaAsN, InAs.

DOI: 10.21883/SC.2022.10.54909.9951

1. Introduction

Due to the small value of chromatic dispersion at a wavelength of 1300 nm in silicon fibers, the use of Vertical Cavity Surface-Emitting Lasers (VCSELs) of this spectral range is the most preferable in terms of increasing the volume and range of data transmission (bandwidth) in comparison with communication lines based on the VCSELs of the spectral range 850−1060 nm.

To date, two main approaches have been used to implement the high-speed VCSELs in the spectral range of 1300 nm. The first approach is to use active regions of InAlGaAs-InP with the formation of a buried tunnel junction (BTJ) for current and optical Confinements, along with the use of high-contrast dielectric distributed Bragg reflectors based on CaF_2/Si [1–3]. The second approach is to use the technology of double wafer fusion [4–8]. In this case, the heterostructure of the active region In(Al)GaAs-InP with BTJ is fused with heterostructures of the upper and lower distributed Bragg reflectors on GaAs substrates, followed by the formation of mesa structures [9].

The creation of monolithic (grown in one epitaxial process) long-wave VCSELs are of the greatest interest for practical applications, however, due to physical and technological limitations, the parameters of these devices are still significantly inferior to the parameters of VCSELs based on the approaches discussed above. The latest results on the metamorphic growth of VCSELs on InP substrates, presented in [10], showed an output optical power of ~ 1.5 mW, which did not allow us to study the modulation characteristics of lasers.

In turn, monolithic VCSELs of the spectral range 1300 nm based on nitrogen-containing active regions on GaAs substrates made it possible to realize higher output characteristics [11–14], and also presented the results of a study of the reliability of this type of VCSEL [15,16]. At the same time, it is worth noting that no significant progress has been demonstrated since the first results on nitrogen-containing VCSELs. In 2008, the frequency of low-signal modulation was implemented at the level of decline of 3 dB $f_{3dB} \sim 10$ GHz (corresponds to 10 Gb/s), the output optical power of P_{out} was 4 mW [11]. In 2020, an increase in the data transfer rate to 12 Gb/s [17] is shown, however, the value of P_{out} was 0.6 mW [11].

The implementation of VCSELs of the spectral range of 1550 nm based on the InGaAsN quantum well (QW) leads to the need to increase the nitrogen composition to 4% and indium to 40%, which leads to the need for further reduction of growth temperatures to 390°C and negatively affects the output characteristics of the devices [18]. Epitaxy at higher temperatures is possible due to the transition from the InGaAsN material system

to InGaAsNSb compounds, however, the characteristics of VCSELs in the spectral range of 1550 nm based on InGaAsNSb QW remain very low (frequency $f_{3dB} \sim 4$ GHz $P_{out} \sim 0.3$ mW [19]) in comparison with the VCSELs of the spectral range 1300 nm based on InGaAsNSb QW [17].

The main reason for the lack of progress in the creation of nitrogen-containing VCSELs on GaAs substrates is the complexity of the growth conditions necessary to obtain nitrogen-containing QWs of high structural quality [20]. An increase in growth temperatures leads to a fluctuation in the composition of the QW along the heterointerface (diffusion effect in the plane of the layers) [21]. Despite the fact that high-temperature annealing of samples reduces the number of nonradiative recombination centers, especially for structures with a nitrogen concentration of $> 1\%$ [22], annealing leads to an undesirable short-wave shift of the emission wavelength [23]. This shift in the emission wavelength and an increase in the intensity of photoluminescence (PL) can be caused by the formation of In-N clusters during high-temperature annealing [24]. Moreover, the effect of flattening of heterointerfaces (increasing the homogeneity of the composition along the QW layer) is not observed [21]. Also, after high-temperature annealing, the effect of indium and gallium interdiffusion between the QW layers and barriers is typical [25] along with the diffusion effect in the plane of layers. To exclude this effect of interdiffusion In-Ga, in some cases additional layers Ga(N)As are used, located between QWs and barriers [26].

In turn, the use of active regions based on short-period superlattices (SLs) consisting of alternating layers of InAs and GaAsN allows minimizing the effect of nitrogen diffusion from the QW [22]. At the same time, the presence of a mini-band in the superlattice, which is located both in the QWs region and in the region of barriers, makes it possible to significantly increase the overlap integral of a standing light wave with a region that amplifies light, and thereby provide a significant increase in the modal gain [5,6,27] compared with heterostructures based on QW. As a consequence, it is to be expected that the creation of VCSELs based on SLs, consisting of alternating layers of InAs and GaAsN, will increase not only the output optical power, but also the speed of nitrogen-containing VCSELs due to potentially greater modal gain.

This paper presents the results of a study of nitrogen-containing active regions based on SLs grown by molecular beam epitaxy (MBE).

2. Experimental samples

During the experiment, active regions based on SLs consisting of alternating layers of InAs and GaAsN were formed by the MBE. Four types of heterostructures (hereinafter structures 1–4) have been studied, which were grown on GaAs (100) substrates. For all structures, the temperature during epitaxy of the SLs layers was 540°C (according to the thermocouple), and the plasma power of the radio frequency nitrogen source was fixed at 400 W, which corresponded to a nitrogen flow of 0.25 standard cubic centimeters. The structure 1 was designed for optical measurements and included a buffer layer of GaAs with a thickness of 200 nm, unalloyed layers of SLs and a covering layer of unalloyed GaAs with a thickness of 50 nm. SL is formed on the basis of 54 alternating layers of GaAsN(2.1%)/InAs with a thickness of 7 nm/0.303 nm (1 monolayer, ML). Immediately after the deposition of the coating layer, a high-temperature annealing of the sample was carried out in an epitaxial chamber at a temperature of 700°C with a duration of 3 min at an excess pressure of arsenic.

Structures 2–4 were designed to study electroluminescence (EL), and therefore epitaxy was performed on GaAs(100) doped substrates with a concentration of $Si(0.8-4.0) \cdot 10^{18}\,cm^{-3}$. The structures 2–4 differed in the design of the layers of the active region. The structure 2 included silicon doped (impurity concentration was $3 \cdot 10^{18}\,cm^{-3}$) the lower contact layer of GaAs with a thickness of 200 nm, the unalloyed layers of SL and the covering layer of unalloyed GaAs with a thickness of 30 nm, as well as the upper contact layer GaAs layer with a total thickness of 200 nm and doped with beryllium along a gradient with a concentration of dopant in the range of $(1-50) \cdot 10^{18}\,cm^{-3}$. The active area is formed on the basis of two types of SLs: 50 alternating layers of GaAsN(1.9%)/InAs with a thickness of 8 nm/0.303 nm and 50 alternating layers of GaAsN(1.5%)/InAs with a thickness of 10 nm/0.303 nm. Immediately after the deposition of the covering layer of GaAs with a thickness of 30 nm, a high-temperature annealing of the sample was carried out in an epitaxial chamber at a temperature of 700°C with a duration of 3 minutes, after which the deposition of the GaAs contact layer was carried out. The design of the structure 3 is identical to the structure 2, taking into account the difference in the layers of the active region, which includes three types of SLs: 54 alternating layers of GaAsN(2.1%)/InAs with a thickness of 7 nm/0.303 nm, 48 alternating layers of GaAsN(1.9%)/InAs with a thickness of 8 nm/0.303 nm and 38 alternating layers of GaAsN(1.5%)/InAs with a thickness of 10 nm/0.303 nm. The design of the structure 4 is identical to the structure 2, taking into account the difference in the layers of the active region, which includes four types of SLs. A detailed description of the structure of 4 is given in Table 1.

To assess the structural quality of the QCD heterostructure, X-ray diffraction analysis and transmission electron microscopy (TEM) methods were used. Measurements of X-ray diffraction swing curves were carried out near the symmetric (004) GaAs reflex on a diffractometer in parallel geometry of the X-ray beam. A tube with rotating copper anode ($\lambda = 0.15406$ nm) is the 6 kW X-ray radiation source. The analysis of X-ray diffraction curves was carried out using the Diffrac.Leptos (Bruker) software package.

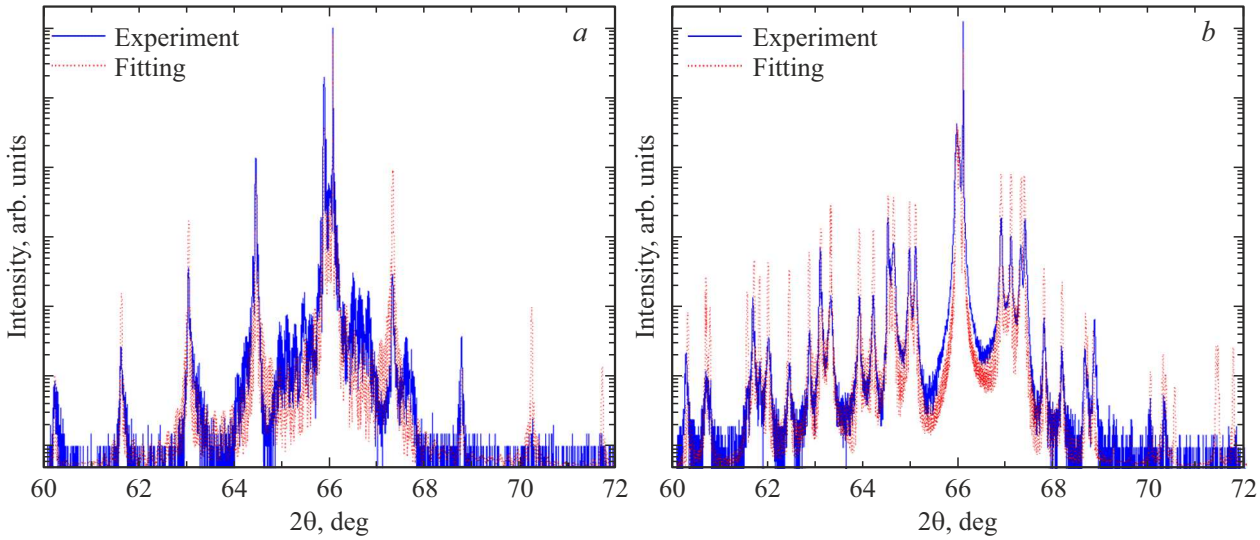

Figure 1. The X-ray diffraction curves of the investigated heterostructures. *a* and *b* — experimental (solid line) and model (dotted line) curves for structure 1 and structure 4, respectively.

Table 1. Description of the heterostructure layers 4. The layers forming the SLs are highlighted in bold

Material	Number repeated layers	Thickness, Å
GaAs	1	2000
GaAs	1	300
InAs GaAsN(1.25%)	32	3.03 120
InAs GaAsN(1.5%)	38	3.03 100
InAs GaAsN(1.9%)	48	3.03 80
InAs GaAsN(2.1%)	54	3.03 70
GaAs	1	2000
Substrate GaAs	1	350 microns

The TEM studies were carried out for structure 4 on a transmission electron microscope JEM2100F (Jeol), located at the Federal Research Center „Materials Science and Diagnostics in Advanced Technologies" Ioffe Institute. A generally accepted method of preparing samples for cross-sectional geometry studies was used: thinning by precision grinding and spraying with argon ions at the final stage before perforation.

Quantitative analysis of the determination of the deep profile of the content of matrix elements nitrogen and indium, as well as beryllium and silicon impurities was carried out for structure 4 using a microprobe secondary ion mass spectrometer (SIMS) with a magnetic sector type mass analyzer with double focusing IMS 7f (Samesa).

Measurements of photoluminescence (PL) spectra at a temperature of 300 K were carried out using an Nd:YLF laser operating in continuous mode to excite the PL. The laser wavelength was 527 nm, the power varied in the range (0.3−3.7) mW, which corresponds to the pump power density of 40−490 kW/cm^2. The PL signal was directed to the input slots of the MS5204i monochromator (Sol Instruments). Detection of the PL spectra was performed using a cooled InGaAs detector (Andor).

To measure the electroluminescence (EL) of the samples, mesas with a diameter of 250 microns were formed by liquid etching through a mask based on layers of upper metallization (Au-Zn), followed by the application of lower metallization to the substrate (Au-Ge). Current pumping was carried out using a 2401 (Keithley) power supply in the current range of 10−100 mA. EL emission was collected from the side wall of the mesa using the lens 20× M Plan Apo NIR (Mitutoyo). To detect the EL spectra at room temperature, a monochromator FHR1000 (Horiba) and an InGaAs CCD-matrix Symphony (Horiba) were used.

3. Results and discussion

Fig. 1 shows experimental X-ray diffraction curves of the swing along with model data for structure 1, which includes one type of SLs, and structure 4, which includes four types of SLs. For the structure 1, a peak from the substrate (maximum intensity) is observed on the XRD curve, as well as a set of satellite peaks characteristic of the periodic structure SLs.

The full width measured at half-height (FWHM) of the satellite peaks was 87−96". According to numerical modeling, the average SLs period was 7.34 nm. Due to the fact

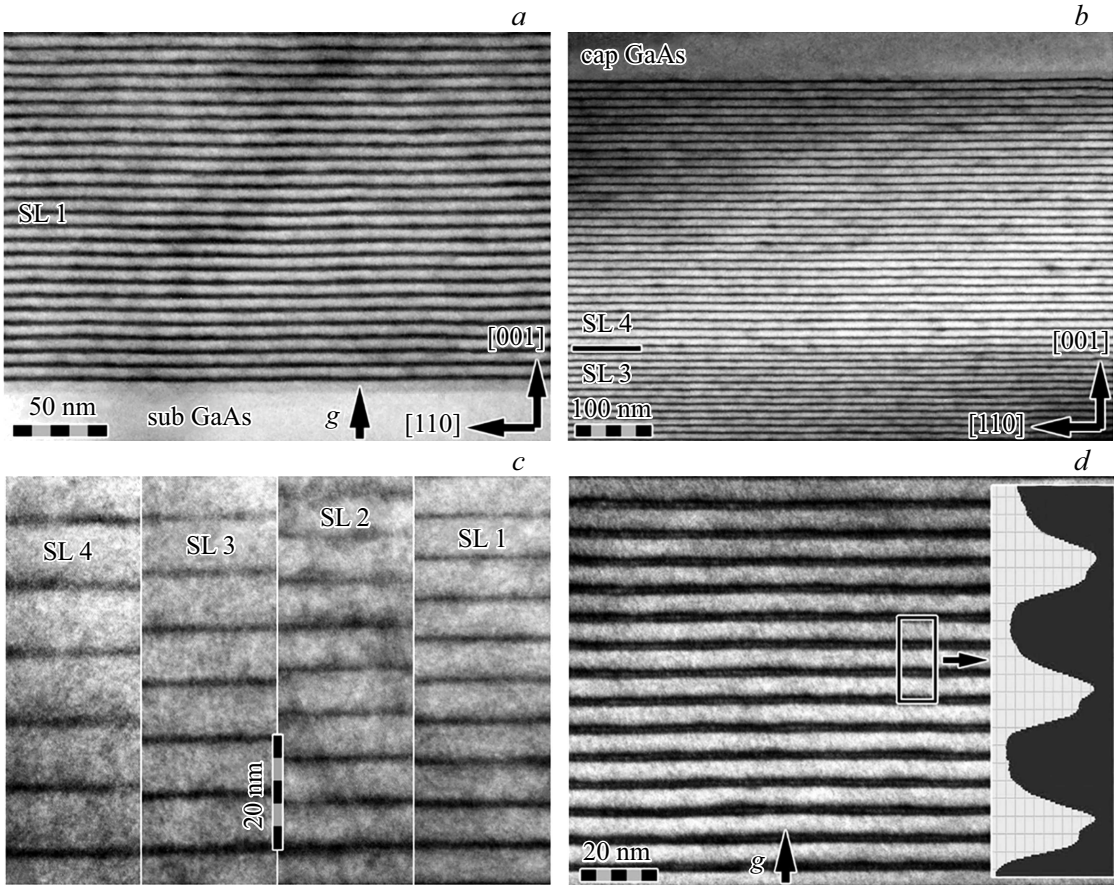

Figure 2. Cross-sectional images $(1-10)$ of the structure 4 obtained from various sites: *a* — near the border with the substrate; *b* — near the border with the upper covering layer; *c* — collage of images from SLs sections of all 4 types; *d* — dark-field image in bi-beam conditions with an active diffraction vector $g = (002)$, sensitive to changes in chemical composition.

that indium and nitrogen introduce mechanical deformations of different signs, it is a very difficult task to determine their individual compositions [28]. In this regard, it seems more reliable to determine the „average" composition of solid alloy layers according to SLs, which according to the simulation results was $In_{0.073}Ga_{0.927}As_{0.981}N_{0.019}$.

For the structure 4, which includes four types of SLs on the XRD curve, there is a peak from the substrate, as well as a set of satellite peaks characteristic of various types of SLs. The FWHM value of the satellite peaks was 96−106". According to numerical modeling, the average period of the four types of SLs was 7.38, 7.90, 9.92 and 11.78 nm, respectively. „Average" composition of layers of solid solutions in four types of SLs, was $In_{0.057}Ga_{0.943}As_{0.985}N_{0.015}$, $In_{0.053}Ga_{0.946}As_{0.986}N_{0.014}$, $In_{0.042}Ga_{0.958}As_{0.988}N_{0.012}$, $In_{0.036}Ga_{0.964}As_{0.991}N_{0.009}$.

The results of studies of the structure 4 by transmission electron microscopy are shown in Fig. 2. The images clearly show the planarity of the GaAsN/InAs layer heteroboundaries both inside each type of SLs (Fig. 2, *c*) and with the substrate (Fig. 2, *a*), as well as with the covering (Fig. 2, *b*) layers. However, it can be noticed that in some places the GaAsN layers corresponding to the darker contrast in the images have slight thickening. One can assume that these thickenings arose due to the nonuniformaty of the diffusion of indium into the surrounding GaAsN during high-temperature annealing at the final stage of fabricating the structure. It was previously shown that the indium diffusion length for the case of epitaxy by the MBE is 1.2 nm [29] in InGaAs/InAlAs; 2.9 nm [30] in InGaAs/GaAs structures. Thus, after high-temperature annealing, the effect of diffusion of indium [31] into the barrier layers is observed, leading to InAs blurring, i.e., to an increase in InAs thickness with a simultaneous decrease in indium content. In all areas available for TEM studies, no extended defects were detected, which confirms the fact that their concentration is smaller than the detection limit, i.e. $< 1 \cdot 10^6$ p/cm^2.

The thickness of the layers was measured using TEM images obtained near the axis of the zone [1–10]. The main difficulty in measuring the thicknesses of thin layers with smooth boundaries was to determine the position of these boundaries. Therefore, the statistical error of such measurements turns out to be greater than the instrumental error of the microscope (5%) and the division price „of the ruler". To measure the thickness of the GaAsN and

Table 2. Results of estimation of average thicknesses in four types of SLs for structure 4

QW Type superlattices	Thickness, nm	Thickness barrier, nm	Thickness period of SLs, nm	Average QW composition	Average layer composition
1	1.3 ± 0.2	6.1 ± 0.31	7.31 ± 0.37	0.32	0.057
2	1.4 ± 0.3	6.6 ± 0.40	7.93 ± 0.40	0.30	0.053
3	1.6 ± 0.3	8.3 ± 0.42	9.84 ± 0.50	0.26	0.042
4	1.7 ± 0.2	10.0 ± 0.50	11.71 ± 0.60	0.25	0.036

InAs layers, an image intensity profile was constructed along the growth direction (perpendicular to the layers) with an averaging width of 10 nm. The boundaries of the layers were determined by the middle of the intensity transition from one layer to the next. The thickness of all layers in one image was measured, then averaged and the average value was determined. The results of measurements of the thickness of the layers are given in Table. 2.

The thickness of the SLs period was calculated by measuring the thickness of the maximum number of periods in one image (10–13), followed by dividing by their number. Thus, the error in determining the boundaries of the layers decreases by an order of magnitude and the main error was the instrumental error of the microscope.

The composition of InGaAs layers was estimated using dark-field TEM images (Fig. 2, *d*) obtained under bi-beam conditions with the effective diffraction vector $g = (002)$. Under these conditions, the intensity of the image is proportional to the square of the difference of the atomic scattering factors of elements in the III and V sublattices and, thus, reflects changes in chemical composition. It is known that the contrast from the layer $In_xGa_{1-x}As$ changes non-linearly with increasing „x“. In the work [32] it is shown that it has a minimum at $x \simeq 0.18$. Having this reference point, an estimate of „x“ in QW was made, which is in the range (0.20–0.35). At the same time, it is impossible to determine the distribution profile of indium from dark-field images, due to the small thickness of the QW.

The results of measurements of the thickness of the QW allow us to conclude that the average thickness of the QW decreases from the surface to the substrate. This fact can be observed if the indium diffusion length turned out to be shorter for deeper layers. Usually, during the MBE growth, heating occurs from the substrate/substrate holder, so it is incorrect to assume that the temperature of the deep layers was lower during the final annealing of 800°C with due to non-equalization of the temperature gradient. Rather, on the contrary, it could be a little bigger. As a result, the activation energy of indium diffusion increased for deep layers due to changes in the properties of the surrounding GaAsN layers, for example, due to a decrease in the concentration of point defects. Since the thickness of the InAs QW turned out to be different, the indium content in them should be greater for thin layers of SLs 1 compared to SLs 4. Using the values of the thicknesses of

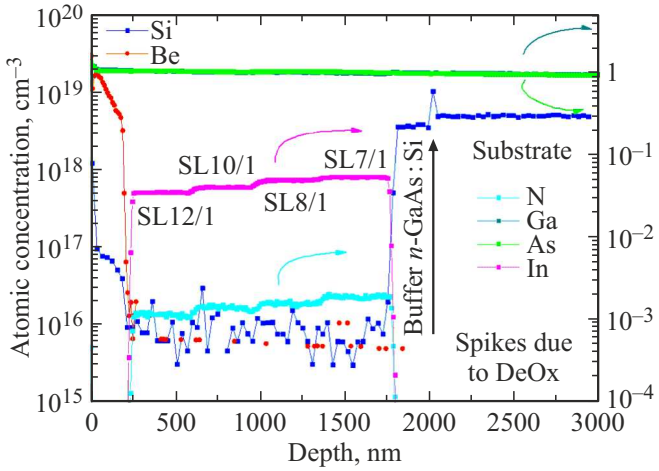

Figure 3. The SIMS depth distribution profile of the epitaxial structure 4 of the content of matrix elements nitrogen and indium and impurities of beryllium and silicon.

the GaAsN/InAs layers from TEM studies and the values of the average SLs compositions obtained by modeling X-ray diffraction curves, it is possible to once again estimate the indium content in the QW. The evaluation results are given in Table 2.

The results of the study by the SIMS-profiling of the depth distribution of the epitaxial structure 4 of the content of matrix elements nitrogen and indium, as well as beryllium and silicon impurities are shown in Fig. 3. No modulation of these values, characteristic of multilayer heterostructures, was found on the dependences of the content of group III elements and nitrogen on the depth of ion etching. The reason for this behavior may be both the roughness of the initial surface of the structure inherited by the bottom of the ion etching crater, comparable in magnitude to the thickness of the narrow-band layer of the superlattice (InAs), and the diffusion of indium from the ultrathin narrow-band layers of the superlattice into its wide-band layers during epitaxial growth and/or during annealing of the structure, discussed above. Previously, the effect of interdiffusion In-Ga in GaInNAs QW, as well as interdiffusion N-As in barrier layers was confirmed by the SIMS method for GaInNAs/GaAs QW-based structures separated by thick barriers [33,34] in comparison with current structures based on SLs GaAsN/InAs.

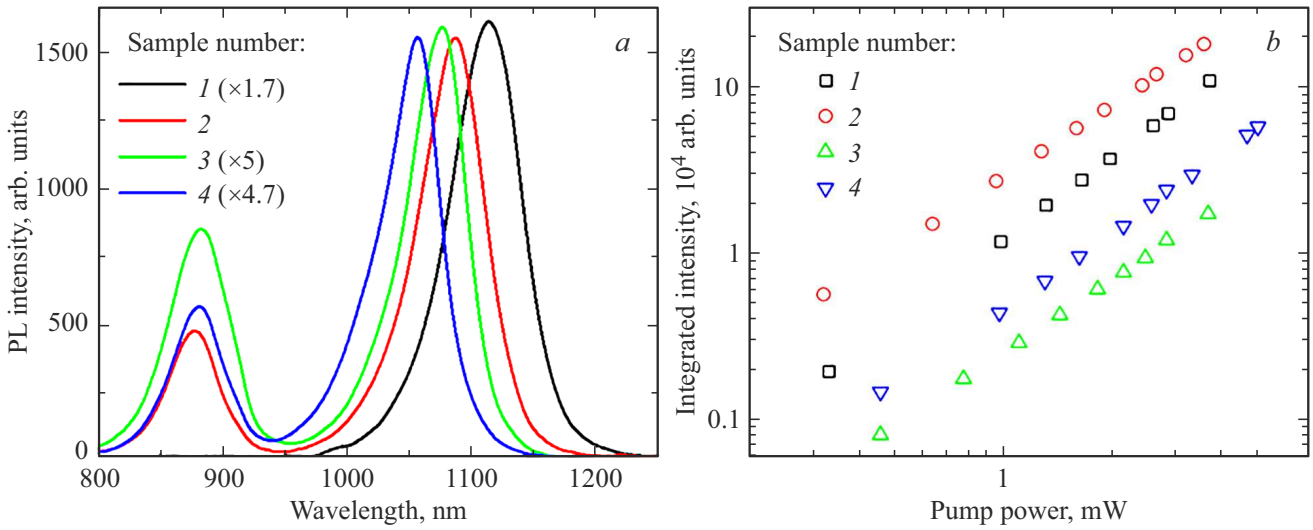

Figure 4. *a* — PL spectra of the structure 1–4, measured at a temperature of 300 K and a pumping power of 2.4 mW; the intensity of the spectra is multiplied by the coefficient shown on the graph for ease of perception; *b* — the dependence of the integral intensity on the pumping power.

Fig. 4, *a* shows the PL spectra of the studied structures obtained at a temperature of 300 K (pumping power density 76.5 kW/cm^2). The line corresponding to the SLs PL is observed in the wavelength range of 950–1200 nm. The maximum intensity of the PL structure 1 is located at a wavelength of 1114 nm. The addition of additional SLs types to the heterostructure in structures 2–4 with an increase in the thickness of the GaAsN barrier layers and a simultaneous decrease in the nitrogen fraction in them leads to a short-wave shift in the position of the maximum PL. The line in the wavelength range 800–950 nm corresponds to the radiation of the contact layer p^+ GaAs. The value of the FHWM of the SLs PL line of structures 1–4 is in the range of 64–75 meV. Earlier, smaller values of the half-width of the peak of the PL were demonstrated for nitrogen-containing active regions (30–37 meV [35] for a set of GaInNAs QW and 18–20 meV for the single QW [36–39]). These values of FWHM are smaller than the magnitude of thermal broadening in the bulk material ($1.8 \times kT$, where k — Boltzmann constant [40], T — temperature), which is due to the type of the density function of states in QW. The presence of a fluctuation of the composition in nitrogen-containing active regions leads to a 2–3 fold increase in the half-width of the PL line in GaInNAs QW in comparison with InGaAs QW [41]. Moreover, an increase in the number of QWs in the active region leads to an additional increase in the fluctuation of the composition and a broadening of the peak of PL in structures based on several QWs. In the case of a set of QWs [42], the total thickness of the active region can be ~ 0.2 microns. The transition to multi-period SLs leads to a further increase in the total thickness of the active region, at least up to 0.4 microns and, as a consequence, to an additional broadening of the line of PL clusters.

With an increase in the pumping power from 0.3 to 3.7 mW, a linear increase in the intensity of PL is observed for each of the structures without any signs of intensity saturation (Fig. 4, *b*). The identical nature of the slope of the obtained dependencies indicates the absence of additional sources of nonradiative recombination in structures 2–4 when using other types of SLs. In addition, the dependence of the maximum position of the PL structures on the optical pumping power is investigated (the obtained dependence on the example of the structure 2 is shown in Fig. 5). At the optical pumping level in the range of 0.02–0.4 mW, the position of the maximum of the PL spectrum practically does not change. As shown earlier [43], the absence of a shift of the radiation wavelength to the short-wavelength

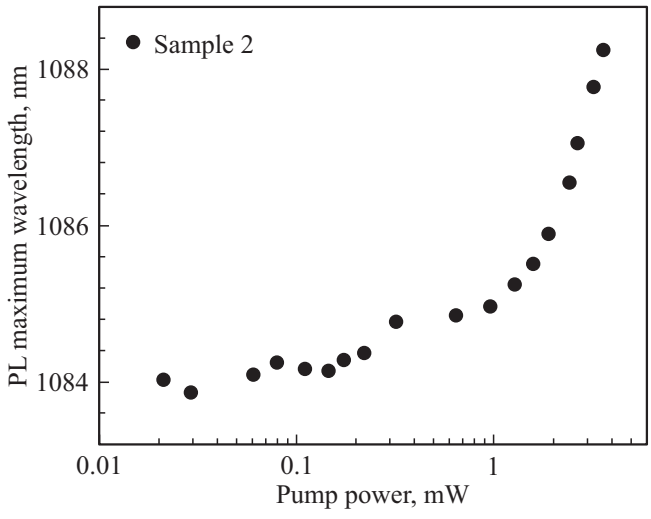

Figure 5. Dependence of the position of the maximum intensity of the PL line on the pumping power for the structure 2.

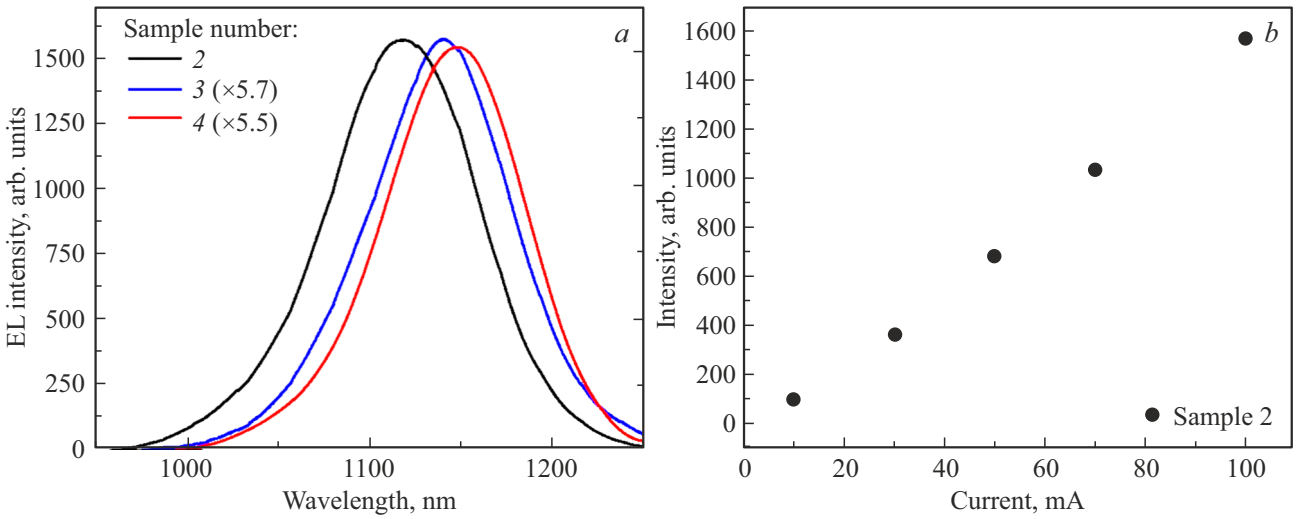

Figure 6. *a* — EL spectra for samples 2–4 at a pump current of 100 Ma, the intensity of the spectra is multiplied by the coefficient shown on the graph for ease of perception; *b* — dependence of the radiation intensity on the pump current for sample 2.

region of the spectrum with an increase in the level of optical pumping, along with the preservation of the half-width of the PL line, may indicate a low level of localization of charge carriers in the studied samples, which can be neglected at room temperature. A further increase in the pumping power leads to a shift in the wavelength of radiation to the long-wavelength region associated with overheating of the structure under the action of laser radiation.

Fig. 6, *a* shows the normalized spectra of EL structures 2–4 at a pump current of 100 mA (corresponds to a current density of 204 A/cm^2). The wavelength of the position of the maximum of the EL spectrum and its half-width for each of the samples did not change with an increase in the pumping current from 10 to 100 mA. Fig. 6, *b* shows the dependence of the EL intensity on the pumping current for the structure 2. The linear nature of this dependence is also observed for other structures.

4. Conclusion

Studies of heterostructures of nitrogen-containing active regions based on multiperiod GaAsN/InAs superlattices created by molecular beam epitaxy have been carried out. The data of X-ray diffraction analysis, as well as the data of TEM studies, confirm the high structural perfection and uniformity of the thicknesses and composition of layers in various parts of the superlattices. At the same time, it is worth noting the presence of the effect of indium interdiffusion from InAs layers after high-temperature annealing of samples. The depth distribution of the epitaxial structure of the content of matrix elements nitrogen and indium, as well as beryllium and silicon impurities, was studied.

Active regions based on GaAsN/InAs superlattices exhibit photoluminescence near 1100 nm with a characteristic half-width of $\sim$ 70 meV. The effective electroluminescence of the studied structures near 1150 nm was demonstrated. Further experiments will be aimed at the realization of nitrogen-containing active regions based on superlattices emitting in the spectral range of 1250–1300 nm due to a systematic change in the ratio of the thicknesses of the GaAsN and InAs layers in the superlattice.

Funding

The work of the authors from the Alferov University was carried out at the expense of a grant from the Russian Science Foundation (project No. 21-19-00718) in terms of design development, epitaxy of heterostructures, TEM and SIMS studies, studies of electroluminescent properties. The work of the authors from ITMO University was carried out with the financial support of the „Priority 2030“ program in terms of the study of X-ray diffraction curves. I.A. Melnichenko and N.A. Fominykh are grateful for the support of the Fundamental Research Program of the National Research University „Higher School of Economics“ regarding the analysis of photoluminescence spectra.

Acknowledgments

The SIMS studies were performed using the IMS 7f (SAMESA) equipment located at the Federal Research Center „Materials Science and Diagnostics in Advanced Technologies“ FTI named after A.F. Ioffe.

Conflict of interest

The authors declare that they have no conflict of interest.

References

[1] R.M. von Wurtemberg, P. Sundgren, J. Berggren, M. Hammar, M. Ghisoni, V. Oscarsson, E. Odling, J. Malmquist. Proc. SPIE (Strasbourg, France, 2004) v. 5453. https://doi.org/10.1117/12.547272

[2] A. Malacarne, C. Neumeyr, W. Soenen, F. Falconi, C. Porzi, T. Aalto, J. Rosskopf, J. Bauwelinckm, A. Bogoni. J. Lightwave Technol., **36** (9), 1527 (2018).

[3] C. Grasse, M. Mueller, T. Gruendl, G. Boehm, E. Roenneberg, P. Wiecha, J. Rosskopf, M. Ortsiefer, R. Meyer, M.C. Amann. J. Cryst. Growth, **370**, 217 (2013).

[4] P. Wolf, H. Li, A. Caliman, A. Mereuta, V. Iakovlev, A. Sirbu, E. Kapon, D. Bimberg. ACS Photonics, **4** (8), 2018 (2017).

[5] S. Blokhin, A. Babichev, A. Gladyshev, L. Karachinsky, I. Novikov, A. Blokhin, S. Rochas, D. Denisov, K. Voropaev, A. Ionov, N. Ledentsov, A. Egorov. Electron. Lett., **57** (18), 697 (2021).

[6] S.A. Blokhin, A.V. Babichev, A.G. Gladyshev, L.Ya. Karachinsky, I.I. Novikov, A. A. Blokhin, M.A. Bobrov, N.A. Maleev, V.V. Andryushkin, D.V. Denisov, K.O. Voropaev, I.O. Zhumaeva, V.M. Ustinov, A.Yu. Egorov, N.N. Ledentsov. IEEE J. Quant. Electron., **58** (2), 1 (2022).

[7] S.A. Blokhin, N. Ledentsov, jr., S.S. Rochas, A.V. Babichev, A.G. Gladyshev, Ł. Chorchos, O.Yu. Makarov, L.Ya. Karachinsky, I.I. Novikov, A.A. Blokhin, M.A. Bobrov, N.A. Maleev, V.V. Andryushkin, K.O. Voropaev, I.O. Zhumaeva, V.M. Ustinov, A.Yu. Egorov, N.N. Ledentsov. In Proc. SPIE (San Francisco, CA, United States, 2022) v. 12020, p. 120200K. https://doi.org/10.1117/12.2605451

[8] S.A. Blokhin, A.V. Babichev, A.G. Gladyshev, I.I. Novikov, A.A. Blokhin, M.A. Bobrov, N.A. Maleev, V.V. Andryushkin, D.V. Denisov, K.O. Voropaev, V.M. Ustinov, V.E. Bougrov, A.Y. Egorov, L.Y. Karachinsky. Opt. Eng., **61** (9), 096109 (2022).

[9] A.V. Babichev, L.Ya. Karachinsky, I.I. Novikov, A.G. Gladyshev, S.A. Blokhin, S. Mikhailov, V. Iakovlev, A. Sirbu, G. Stepniak, L. Chorchos, J.P. Turkiewicz, K.O. Voropaev, A.S. Ionov, M. Agustin, N.N. Ledentsov, A.Yu. Egorov. IEEE J. Quant. Electron., **53** (6), 1 (2017).

[10] Y. Ohiso, T. Sato, T. Shindo, H. Matsuzaki. Electron. Lett., **56** (2), 95 (2020).

[11] Y. Onishi, N. Saga, K. Koyama, H. Doi, T. Ishizuka, T. Yamada, K. Fujii, H. Mori, J.-I. Hashimoto, M. Shimazu, A. Yamaguchi, T. Katsuyama. IEEE J. Select. Top. Quant. Electron., **15** (3), 838 (2009).

[12] J. Vukusic, P. Modh, A. Larsson, M. Hammar, S. Mogg, U. Christiansson, V. Oscarsson, E. Ödling, J. Malmquist, M. Ghisoni, P. Gong, E. Griffiths, A. Joel. Electron. Lett., **39** (8), 662 (2003).

[13] H. Riechert, A. Ramakrishnan, G. Steinle. Semicond. Sci. Technol., **17** (8), 892 (2002).

[14] G. Steinle, H. Riechert, A. Y. Egorov. Electron. Lett., **37** (2), 93 (2001).

[15] D.W. Kisker, L.M.F. Chirovsky, R.L. Naone, J.M. Van Hove, J.M. Rossler, M. Adamcyk, N. Wasinger, J.G. Beltran, D. Galt. In Proc. SPIE (San Jose, CA, United States, 2004) v. 5364. https://doi.org/10.1117/12.539285

[16] S.R. Prakash, L.M.F. Chirovsky, R.L. Naone, D. Galt, D.W. Kisker, A.W. Jackson. In Proc. SPIE (San Jose, CA, United States, 2003) v. 4994. https://doi.org/10.1117/12.482853

[17] M. G[e]bski, D. Dontsova, N. Haghighi, K. Nunna, R. Yanka, A. Johnson, R. Pelzel, J.A. Lott. OSA Continuum, **3** (7), 1952 (2020).

[18] J.S. Harris, H. Bae, T. Sarmiento. GaInNAs(Sb) *Long-Wavelength VCSELs, VCSELs: Fundamentals, Technology and Applications of Vertical-Cavity Surface-Emitting Lasers*, ed. by R. Michalzik (Berlin–Heidelberg, Springer Verlag, 2013) p. 353–377.

[19] T. Sarmiento, L. Zhao, P. Moser, T. Li, Y. Huo, J.S. Harris. IEEE Phot. Technol. Lett., **31** (20), 1607 (2019).

[20] R. Fehse, S. Tomic, A.R. Adams, S.J. Sweeney, E.P. O'Reilly, A. Andreev, H. Riechert. IEEE J. Select. Top. Quant. Electron., **8** (4), 801 (2002).

[21] L. Geelhaar, M. Galluppi, G. Jaschke, R. Averbeck, H. Riechert, T. Remmele, M. Albrecht, M. Dworzak, R. Hildebrant, A. Hoffmann. Appl. Phys. Lett., **88** (1), 011903 (2006).

[22] M. Albrecht, V. Grillo, T. Remmele, H.P. Strunk, A.Yu. Egorov, Gh. Dumitras, H. Riechert, A. Kaschner, R. Heitz, A. Hoffmann. Appl. Phys. Lett., **81** (15), 2719 (2002).

[23] L. Geelhaar, M. Galluppi, R. Averbeck, G. Jaschke, H. Riechert. Appl. Phys. Lett., **90** (7), 071913 (2007).

[24] M. Albrecht, T. Remmele, V. Grillo, H.P. Strunk, A. Kaschner, A. Hoffmann, A. Egorov, H. Riechert. In 2003 Int. Symp. on Compound Semiconductors (San Diego, CA, USA, 2003). https://doi.org/10.1109/ISCS.2003.1239907

[25] H.D. Sun, R. Macaluso, M.D. Dawson, F. Robert, A.C. Bryce, J.H. Marsh, H. Riechert. J. Appl. Phys., **94** (3), 1550 (2003).

[26] S. Govindaraju, J.M. Reifsnider, M.M. Oye, A.L. Holmes. J. Electron. Mater., **33** (8), 851 (2004).

[27] N.V. Kryzhanovskaya, A.I. Likhachev, S.A. Blokhin, A.A. Blokhin, E.V. Pirogov, M.S. Sobolev, A.V. Babichev, A.G. Gladyshev, L.Ya. Karachinsky, I.I. Novikov, V.V. Andryushkin. Laser Phys. Lett., **19** (7), 075801 (2022).

[28] V. Grillo, M. Albrecht, T. Remmele, H.P. Strunk, A.Yu. Egorov, H. Riechert. J. Appl. Phys., **90** (8), 3792 (2001).

[29] K. Muraki, S. Fukatsu, Y. Shiraki, R. Ito. Appl. Phys. Lett., **61** (5), 557 (1992).

[30] P. Offermans, P.M. Koenraad, J.H. Wolter, M. Beck, T. Aellen, J. Faist. Appl. Phys. Lett., **83** (20), 4131 (2003).

[31] C.A. Wang, B. Schwarz, D.F. Siriani, L.J. Missaggia, M.K. Connors, T.S. Mansuripur, D.R. Calawa, D. McNulty, M. Nickerson, J.P. Donnelly, K. Creedon, F. Capasso. IEEE J. Select. Top. Quant. Electron., **23** (6), 1 (2017).

[32] A. Lemaître, G. Patriarche, F. Glas. Appl. Phys. Lett., **85** (17), 3717 (2004).

[33] R. Macaluso, H.D. Sun, M.D. Dawson, F. Robert, A.C. Bryce, J.H. Marsh, H. Riechert. Appl. Phys. Lett., **82** (24), 4259 (2003).

[34] H.D. Sun, R. Macaluso, S. Calvez, M.D. Dawson, F. Robert, A.C. Bryce, J.H. Marsh, P. Gilet, L. Grenouillet, A. Million, K.B. Nam, J.Y. Lin, H.X. Jiang. J. Appl. Phys., **94** (12), 7581 (2003).

[35] A. Kaschner, T. Lüttgert, H. Born, A. Hoffmann, A.Yu. Egorov, H. Riechert. Appl. Phys. Lett., **78** (10), 1391 (2001).

[36] S. Shirakata, M. Kondow, T. Kitatani. Appl. Phys. Lett., **80** (12), 2087 (2002).

[37] S. Shirakata, M. Kondow, T. Kitatani. Appl. Phys. Lett., **79** (1), 54 (2001).

[38] T. Kitatani, M. Kondow, T. Tanaka. J. Cryst. Growth, **227–228**, 521 (2001).

[39] S. Zhang, Z. Niu, H. Ni, D. Wu, Z. He, Z. Sun, Q. Han, R. Wu. Appl. Phys. Lett., **87** (16), 161911 (2005).
[40] E. Fred Schubert. *Light-Emitting Diodes* (Cambridge, England, Cambridge University Press, 2006) p. 217. https://doi.org/10.1017/CBO9780511790546
[41] G. Dumitras, H. Riechert, H. Porteanu, F. Koch. Phys. Rev. B, **66** (20), 205324 (2002)
[42] A.Yu. Egorov, D. Bernklau, D. Livshits, V. Ustinov, Zh.I. Alferov, H. Riechert. Electron. Lett., **35** (19), 1643 (1999).
[43] G. Jaschke, R. Averbeck, L. Geelhaar, H. Riechert. J. Cryst. Growth, **278** (1−4) 224 (2005).